

See discussions, stats, and author profiles for this publication at: <https://www.researchgate.net/publication/263953890>

Pathway Complexity in π -Conjugated Materials

ARTICLE *in* CHEMISTRY OF MATERIALS · SEPTEMBER 2013

Impact Factor: 8.35 · DOI: 10.1021/cm4021172

CITATIONS

25

READS

28

3 AUTHORS, INCLUDING:



Peter Korevaar

Harvard University

17 PUBLICATIONS 390 CITATIONS

[SEE PROFILE](#)



Tom F. A. de Greef

Technische Universiteit Eindhoven

60 PUBLICATIONS 2,447 CITATIONS

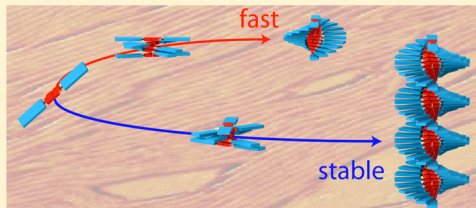
[SEE PROFILE](#)

Pathway Complexity in π -Conjugated Materials

Peter A. Korevaar,^{†,‡} Tom F. A. de Greef,^{†,§} and E. W. Meijer^{*,†,‡}

[†]Institute for Complex Molecular Systems, [‡]Laboratory of Macromolecular and Organic Chemistry, and [§]Computational Biology, Eindhoven University of Technology, P.O. Box 513, 5600 MB Eindhoven, The Netherlands

ABSTRACT: To arrive at functional organic materials with optimal molecular organization, control over the aggregation process is a prerequisite. Often, however, multiple pathways are involved that compete for the same molecular building block, a phenomenon known as pathway complexity. As a result, the material—made from small molecules or polymers—can get entrapped in a metastable pathway while a more stable but slower formed morphology is aimed for. Vice versa, the equilibrium state can be obtained easily, but another, less stable morphology is desired as it has more interesting properties. In both cases, the solution processing, starting from molecularly dissolved material, should be optimized to select the desired aggregation pathway. This Perspective aims to outline the importance of mechanistic insights derived from self-assembly of 1D fibers in diluted solutions to unravel and control aggregation pathways involved in the processing of π -conjugated materials.



KEYWORDS: metastable morphologies, solution processing, pathway selection, self-assembly, modeling

1. INTRODUCTION

Control over the nanoscale organization of π -conjugated molecules is regarded as one of the key parameters in the performance of organic electronic devices.^{1–7} To obtain the best characteristics, such as high charge-carrier mobility for field effect transistors (FET) or efficient electron–hole separation in bulk heterojunction (BHJ) solar cells, every atom has to be placed at the optimal position in three-dimensional space. The design of individual molecules—either small molecules or polymers—is often straightforward as both theories to predict the electronic properties of the molecular building blocks and synthetic methodologies to obtain them in pure form have reached an exceptional level of sophistication. However, control on the next length scale, beyond the molecular formula, is much more complicated, and finding self-assembly pathways which yield optimal molecular organization is still an endeavor that mainly relies on a trial-and-error approach.¹

The common strategy in the processing of π -conjugated materials is to start with conditions where the molecules or polymers are completely, i.e., “molecularly” dissolved. This can be achieved by addition of a good solvent like chloroform in combination with elevated temperatures. Next, the onset of aggregation is induced by changing the solvent conditions, for instance by spin coating or adding a solvent in which the molecules are less soluble (i.e., poor solvent). However, the outcome of the aggregation process is often dependent on the processing methodology, meaning that different preparation protocols attenuate different aggregation pathways and consequently result in different nanoscale morphologies. Obviously, since the performance of functional devices depends on an optimal morphology, unraveling clear relations between processing methodology and pathway selection is of great interest for this field of research. Therefore, it is not surprising to see a large number of articles^{8–21} and excellent reviews^{22,23}

recently addressing the need to control the self-assembly pathways of π -conjugated materials.

The influence of the aggregation pathways on the molecular organization of functional π -conjugated materials emphasizes the importance of mechanistic insights into molecular self-assembly. In the field of chemical self-assembly, the aggregation of small molecules—including π -conjugated monomers—into one-dimensional fibers is studied in detail. In this perspective, we point out that mechanistic insights into aggregation pathways of π -conjugated molecules, as obtained via studies on their molecular self-assembly, can be highly valuable to understand and optimize the processing of π -conjugated functional materials. We demonstrate the analogy between pathway complexity, i.e., the competition of multiple aggregation pathways for the molecular building blocks, in bulk materials and one-dimensional nanofibers. Next we discuss kinetic models to describe nucleated one-dimensional self-assembly, starting with a single pathway system and then expanding the analysis with a model in which also metastable structures are incorporated. Finally we demonstrate, using an example from our own work, how multiple aggregation pathways can be recognized and selected.

2. METASTABLE MORPHOLOGIES

Metastable morphologies that are formed in the initial aggregation stages of π -conjugated molecules can have major effects on the subsequent self-assembly process. Often, these spurious, metastable structures act as a trap for the molecular

Special Issue: Celebrating Twenty-Five Years of Chemistry of Materials

Received: June 29, 2013

Revised: August 20, 2013

Published: August 21, 2013

building blocks, and due to this entrapment the formation of the desired morphology is retarded or even made impossible at reasonable time-scales. In other cases, however, the metastable structure has superior properties compared to equilibrium aggregates, and hence the preparation protocol should be optimized to favor the metastable pathway while making sure that the nanostructures do not re-equilibrate back to other, lower energy morphologies. In this section, we discuss the influence of kinetic pathways both for π -conjugated materials as well as the molecular assembly of one-dimensional fibers in diluted solution. It should be mentioned that the selection of examples is not meant to provide a full overview of the field, but rather to illustrate the phenomenon of pathway complexity as well as its consequences in engineering functional molecular nanostructures.

Metastability in π -Conjugated Materials. To probe the molecular organization of π -conjugated polymers or oligomers, the material can be functionalized with chiral side chains and studied with circular dichroism (CD) spectroscopy. The introduction of stereocenters serves as a spectroscopic label since the magnitude and sign of CD spectra are very sensitive to optical transitions, either within the twisted π -conjugated backbone or in helical aggregates formed by multiple polymer chains. One of the first examples of a chiral π -conjugated polymer that displays different CD spectra upon different preparation protocols is S-chiral polythiophene **1** (Figure 1), as

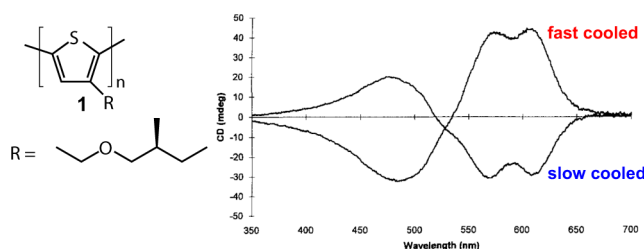


Figure 1. Opposite Cotton effects of chiral polythiophene **1** in thin films reveal multiple aggregation pathways upon fast and slow cooling respectively. (Reprinted with permission from ref 24. Copyright 1995 John Wiley & Sons Inc.)

reported by Bouman and Meijer.²⁴ Spin coated films of **1** on glass reveal a bisignated, negative Cotton effect at room temperature, which is erased upon heating the polymer up to 160 °C. Subsequent cooling results in a reappearance of a helical morphology. However, the sign of the Cotton effect depends on the cooling rate applied: whereas slow cooling yields a negative Cotton effect, quenching the sample in a water bath at 0 °C yields a completely opposite Cotton effect. Only heating the material and cooling slowly results in a reestablishment of the negative Cotton effect. This suggests that fast cooling results in a direct conversion toward metastable aggregates with opposite handedness compared to the thermodynamically stable form that is obtained upon slow cooling.

Another illustrative example of kinetically entrapped morphologies that can be obtained by manipulating the preparation method is reported by Swager and co-workers in the aggregation of poly(*p*-phenylene vinylene), PPV.^{25,26} CD studies on S-chiral PPV **2** in pure chloroform yield no Cotton effect, and hence no helical aggregates are present in this solvent. However, addition of acetonitrile (MeCN) results in a strong bisignate Cotton effect, indicating exciton coupling

between adjacent PPV backbone chains within the aggregates formed. Remarkably, if less than 50% MeCN is added, a positive Cotton effect is obtained, whereas adding more than 50% MeCN yields a negative Cotton effect. Furthermore, the positive Cotton effect can also be obtained if the polymer is dissolved in 1,2-dichloroethane (DCE). Spin coating the aggregate-free solution of PPV in pure chloroform results in a film without any net chiral organization, as indicated by the absence of a Cotton effect. However, after annealing the film at 45 °C in the presence of a chloroform vapor, a negative Cotton effect is obtained. This means that the initially disordered polymer chains reorganize into a chiral morphology that is thermodynamically more stable. Also if PPV is spin coated from DCE, the structures initially present in solution are preserved in the bulk state, as evident from the positive Cotton effect of thin films. However, in this case thermal annealing in the presence of either DCE vapor, chloroform vapor, or an inert nitrogen atmosphere does not affect the helicity of the aggregates. These results, as schematically represented in Figure 2, make clear that

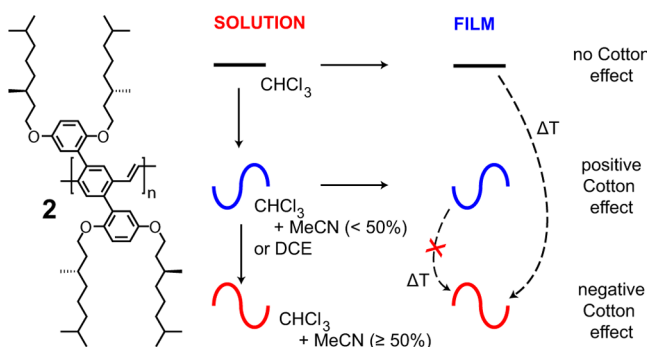


Figure 2. Schematic representation of the diversity of Cotton effects obtained for S-chiral poly(*p*-phenylene vinylene) **2** under different conditions in solution and film.

by spin coating from different solvents, different pathways can be selected toward morphologies with opposite helicities. Even though in the film only one type can be the most stable state, both pathways result in stable structures that do not interconvert at reasonable time scales.

Whereas π -conjugated polymers in most cases fail to crystallize completely and result in a material that contains both crystalline and amorphous domains, small molecules crystallize much easier and often completely. However, in many crystallization processes multiple molecular organizations can be realized, resulting in different crystal structures called polymorphs. In a recent example by Stupp and co-workers, control over the different polymorphs is obtained by taking advantage of the differences in growth kinetics between multiple aggregation pathways.^{27,28} The molecule of interest, quarterthiophene **3**, is molecularly dissolved in the hydrogen-bond accepting solvent tetrahydrofuran (THF), whereas aggregation occurs in toluene. To obtain a solvent that dissolves **3** and can induce its aggregation by slow evaporation or addition of more toluene, a mixture of dioxane, THF, and toluene in a 2:1:1 ratio is applied. Drop casting 10 μ L of **3** (2.5 wt %) in the solvent mixture on a Teflon sheet results in the formation of a network of fibers (Figure 3a). If, however, the evaporation is retarded by the presence of toluene vapor, the same experiment yields rhombohedra structures, the second polymorph. Moreover, a third pathway toward hexagonal prisms can be selected by evaporating a more concentrated

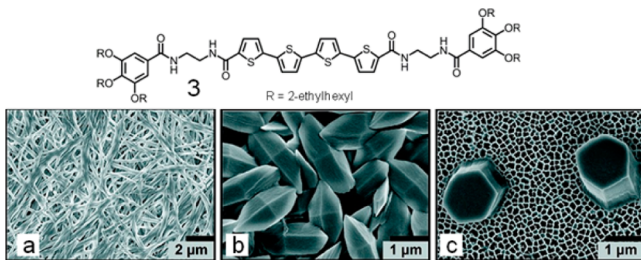


Figure 3. Scanning electron microscopy (SEM) images of the fiber (a), rhombohedra (b), and hexagonal prism (c) morphologies that are obtained for quarterthiophene 3 upon different preparation methods. (Reprinted with permission from ref 27. Copyright 2011 American Chemical Society.)

solution (5 wt %) in the presence of toluene vapor. However, in both cases also fibers are formed next to the rhombohedra and hexagonal prisms, respectively. The fact that fast evaporation yields fibers exclusively suggests that these fibers are formed first and thereafter—if the solvent does not evaporate too fast—convert into a more stable polymorph. Hence, to obtain the exclusive growth of these polymorphs, the aggregation process is slowed down via diffusion of toluene as poor solvent into molecularly dissolved 3. To retard this diffusion, a membrane is applied as a diffusion barrier, and the viscosity of the toluene phase is increased by dissolving poly(methyl methacrylate). The viscous toluene phase is placed on one side of the vertically oriented membrane, and a 5 wt % solution of 3 in 2:1:1 dioxane/THF/toluene on the other side. After diffusion of both solutions into each other and evaporating the solvent, hexagonal prisms are obtained (Figure 3c), whereas the same experiment with a 2.5 wt % solution yields rhombohedra (Figure 3b). Next to the differences between these polymorphs that appear on the micrometer-scale (Figure 3), two-dimensional grazing incidence small-angle X-ray scattering (2D-GISAXS) revealed significant differences in molecular organization as well. Whereas the rhombohedra are found mostly at the bottom of the dried membrane, the hexagonal prisms are all anchored perpendicular to the surface of the membrane. The involvement of the surface in the growth of the hexagonal prisms suggests a heterogeneous nucleation pathway for this polymorph, whereas rhombohedra are formed via homogeneous nucleation.

An elegant methodology to attenuate different self-assembly pathways resulting in a metastable polymorph was reported recently by Bao and co-workers in their studies on the crystallization of pentacene derivative 4 into an organic semiconducting material.²⁹ A special solution-shearing process is applied in which a shearing plate drags a solution of 4 in toluene across a heated substrate (Figure 4). The resulting morphology of the thin film is dependent on the shearing speed. Slow shearing (0.4–2.8 mm/s) results in crystal rods oriented along the shearing direction. For higher shearing rates, the morphology changes from comet-shaped, transcrystalline structures (4 mm/s) to a completely isotropic, spherulitic film (8 mm/s), meaning that the orientation along the shearing direction disappears. Apart from these differences in morphology on the submillimeter scale, the shearing rate also influences the molecular packing. Grazing incidence X-ray diffraction (GIXD) experiments reveal that the shortest π – π distance obtained in a film prepared with a shearing rate of 8 mm/s

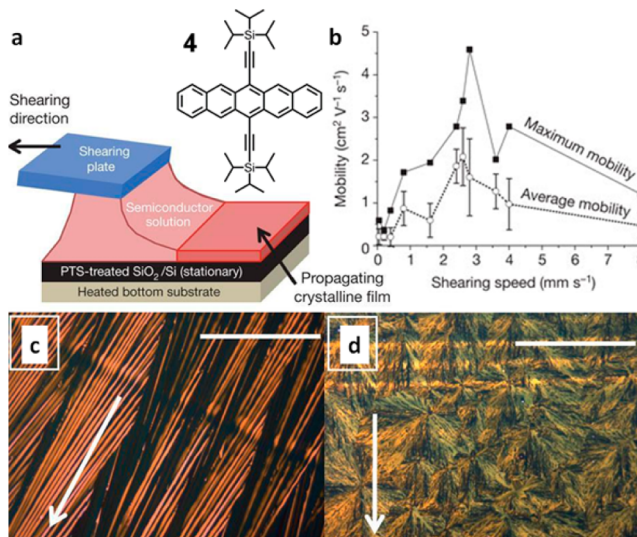


Figure 4. (a) Schematic representation of the solution-shearing process by which the charge carrier mobility in crystals of pentacene derivative 4 can be optimized (b). (c, d) Shearing results in metastable crystals with a higher conductance compared to bulk, equilibrium crystals. However, this effect is counteracted by a loss in anisotropy if the shear speed is too fast (c, shear speed 1.6 mm/s; d, 8 mm/s, scale bars are 200 μ m). (Reprinted with permission from ref 29. Copyright 2011 Nature Publishing Group.)

equals 3.08 Å, whereas π – π distances of 3.33 Å are obtained for films prepared upon evaporation (i.e., no shearing) and in the bulk crystal. Due to this reduction in π – π distance, the charge carrier mobility increases significantly. Thin films prepared with a shearing rate of 2.6 mm/s show an optimum average mobility of $2.1 \text{ cm}^2 \text{ V}^{-1} \text{ s}^{-1}$ along the shearing direction. Although faster shearing rates yield a reduced π – π distance as well, the advantageous effect of this reduction is counteracted by the loss of crystal orientation along the shearing direction. The thin films do not degrade in time and are thermally stable up to 160 °C. However, exposing the film to toluene vapor yields a relaxation of the decreased π – π distance back to the bulk crystal morphology and a concomitant decrease in charge carrier mobility. This indicates that the solution-shearing process directs the aggregation process into a metastable morphology. As the processing methodology starts from a thin liquid film that allows fast solvent evaporation, it is hypothesized that the growing crystal front is given only limited time to crystallize. Hence, the material gets kinetically entrapped in a metastable state with superior properties compared to the equilibrium morphology.

Metastability in π -Conjugated Fibers in Solution. Aida and co-workers assembled graphitic nanotubes with semiconducting properties from hexa-*peri*-hexabenzocoronenes (HBC, 5, Figure 5a).³⁰ These nanotubes can become micrometers long but have a very uniform diameter of 20 nm. The wall of the tubes consists of a 3 nm thick bilayer of π -stacked HBCs, facilitated by the amphiphilic character of the HBC molecule that has two aliphatic dodecyl tails on one side and two hydrophilic triethylene glycol chains on the other. Assembly of HBC 5 in pure THF results in exclusive formation of nanotubes. However, in the presence of 20 vol % water in THF, also helical coils are obtained next to the nanotubes. These coils, comprising helically folded bilayer ribbons, are considered as the topological precursor for the nanotubes,

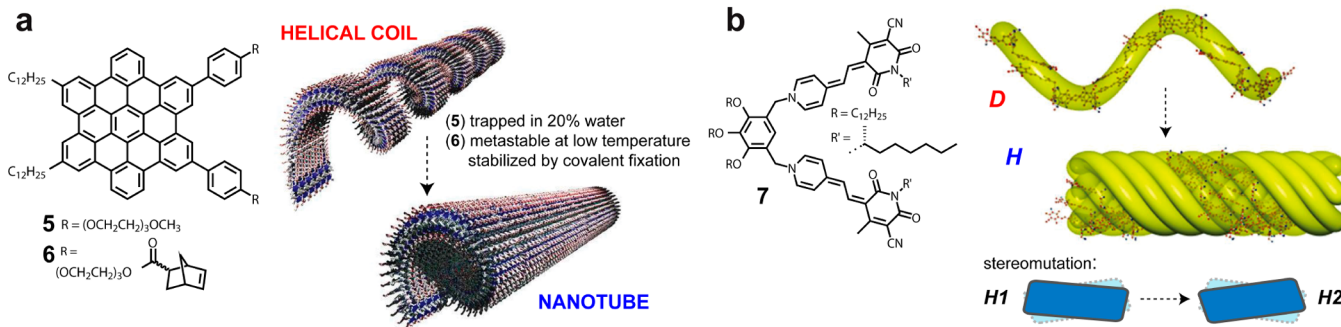


Figure 5. (a) Hexabenzocoronene (HBC) derivatives **5** and **6** assemble under equilibrium conditions in nanotubes. However, HBC **5** can be trapped in metastable helical coils upon addition of 20% water to the solution, whereas for HBC **6** these coils can be obtained at low temperature and thereafter stabilized by covalent fixation upon polymerization of the norbornene groups. (b) Hierarchical assembly process of bismerocyanine **7** into subsequently oligomer chains (**D**) and helical rods (**H**). The helical organization of the merocyanine units in these rods inverts in time, from metastable **H1** to stable **H2**. (Reprinted with permission from ref 31. Copyright 2005 National Academy of Sciences. Reprinted with permission from ref 33. Copyright 2003 John Wiley & Sons, Inc.)

suggesting that they are only kinetically stable.³¹ To further investigate the different structures involved in the HBC assembly pathways, HBC **6** is functionalized with two polymerizable norbornene groups to the triethylene glycol chains.³² Diffusion of diethylether vapor into a solution of **6** in dichloromethane at 25 °C yields nanotubes, whereas vapor diffusion at 15 °C results in helical coils only. The metastable character of these coils is demonstrated by annealing them at 25 °C, which results in a gradual transformation into nanotubes. To stabilize the nanocoils that are only kinetically stable at low temperatures, the norbornene groups are polymerized using a Grubbs catalyst. Whereas nonpolymerized assemblies are disrupted completely, covalently fixed nanocoils maintain their structure up to 75 °C, clearly indicating the stabilizing effect of covalent fixation on the metastable architectures.

The hierarchical assembly pathways of bismerocyanine **7** are studied in detail by Würthner and co-workers.^{33–35} The two merocyanine units of this V-shaped molecule have a large dipole moment that allows both of them to dimerize with the merocyanine unit of another molecule, resulting in randomly oriented oligomer chains (**D** aggregates). In apolar solvents like methylcyclohexane (MCH), these chains assemble further into helical rods (**H** aggregates) that consist of six intertwined chains (Figure 5b). These intertwined chains are visible from atomic force microscopy (AFM) and cryo-transmission electron microscopy (cryo-TEM) while molecular simulations have provided insight into the number of intertwined chains. To rationalize this hierarchical assembly process, a kinetic experiment is performed. Molecularly dissolved **7** in THF is added to MCH, yielding a 30:70 v/v THF/MCH solution. Time-dependent UV-vis spectroscopy reveals the transition from instantaneously assembled **D** aggregates into **H** aggregates. Together with the rise of **H** aggregates, a strong negative Cotton effect appears in the CD spectra, indicative for a helical organization of the chromophores within the intertwined chains of the helical rods. Surprisingly, however, the assembly process proceeds after the appearance of the negative Cotton effect as revealed by a total inversion of the CD spectrum. This stereomutation indicates that the initially formed **H** aggregates, referred to as **H1**, are metastable and reorganize in time into a more stable structure **H2** that has an opposite Cotton effect. To understand this process further, the **D** → **H1** → **H2** conversions are studied using AFM on solutions spin coated

in different stages of the assembly process. Right-handed structures appear in the AFM micrographs for **H1** aggregates corresponding to the structure with a negative Cotton effect. Remarkably, AFM on dried fibers corresponding to **H2** aggregates also show this handedness, even though for this state an opposite Cotton effect is observed. To rationalize these results, it is hypothesized that the helicity of the intertwined chains is not affected during the conversion from **H1** to **H2** aggregates. Only the molecular organization of the merocyanine units within these chains—which is responsible for the sign of the Cotton effect—shifts from a left- to a right-handed fashion. Applying a higher fraction of MCH delays the **H1** → **H2** conversion and results in entrapment of **H1** aggregates for weeks. This suggests that (re)-dissolved molecules play an important role in the stereomutation process from metastable to stable assemblies.

3. MECHANISTIC INSIGHTS

The examples discussed in the previous section make clear that metastable morphologies appear frequently in π -conjugated materials. Avoiding or attenuating entrapment of material in these metastable nanostructures requires in-depth understanding of the individual pathways as well as their mutual interactions. In this respect, we propose that every pathway can be simplified to a one-dimensional aggregation process that (often) starts with a nucleation event. Here, the building blocks are individual molecules in the case of small molecule systems and oligomer segments for polymer systems.^{36–38} The onset of the aggregation process can be described as a purely one-dimensional (1D) assembly process where all monomers stack on top of each other into a fiber, driven by π - π stacking. Alternatively, a fiber can be formed via lateral growth of multiple stacks, as illustrated in Figure 6. It should be mentioned that processing of π -conjugated materials occurs in concentrated solutions and involves multiple aggregation steps beyond the formation of these fiber structures. However, we believe that mechanistic insights derived from assembly of fibers under dilute conditions hold important lessons to unravel and control aggregation pathways in π -conjugated materials. To this end, we will focus in this section on the mechanisms of one-dimensional and lateral assembly processes.

Self-Assembly under Equilibrium Conditions. Self-assembly processes can be described under equilibrium conditions as a sequence of monomer association equilibria,

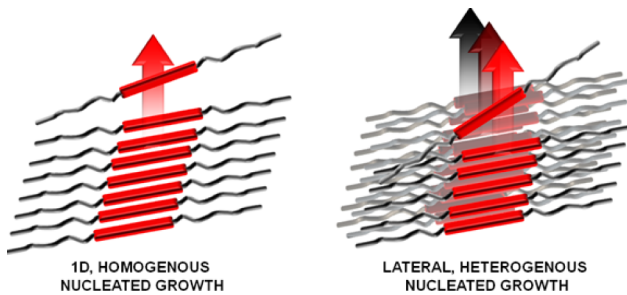


Figure 6. Schematic representation of 1D, homogeneous (left) and lateral, heterogeneous nucleated growth (right).

as depicted in Figure 7. Two major classes of self-assembly mechanisms are the isodesmic and cooperative mechanism.^{39,40}

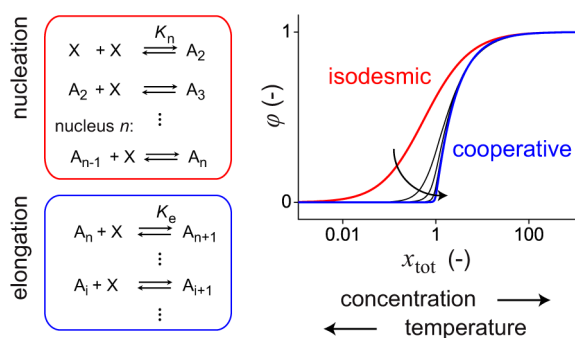


Figure 7. Thermodynamic model for assembly, as developed by Goldstein and Stryer,⁴¹ that describes the assembly of monomer X via a sequence of monomer association equilibria into assemblies A_i . The degree of aggregation φ increases gradually with the dimensionless concentration x_{tot} for isodesmic assembly, and a critical transition at $x_{\text{tot}} = 1$ is obtained for cooperative assembly.

Whereas in isodesmic assembly the monomer association equilibrium constant K is independent of the chain length i ,

cooperative assembly starts with a relatively unfavorable nucleation up to nucleus size n , followed by more favorable elongation. Hence, the equilibrium constant of nucleation K_n is smaller than the equilibrium constant of elongation K_e , and this difference is characterized by the cooperativity $\sigma = K_n/K_e$. Via analysis of the monomer association equilibria, as demonstrated by Goldstein and Stryer,⁴¹ the characteristic features of isodesmic and cooperative assembly can be reconstructed. To this end, the dimensionless concentration $x_{\text{tot}} = K_e \cdot c_{\text{tot}}$ is defined. The dimensionless quantity x_{tot} increases with total concentration c_{tot} and, as the assembly of most π -conjugated systems in nonaqueous solutions is enthalpy driven, decreases with temperature. In Figure 7, the degree of aggregation φ , which equals the fraction of material in aggregates larger than the monomer ($i \geq 2$) for an isodesmic system or aggregates larger than the nucleus ($i > n$) for a cooperative system, is analyzed as a function of x_{tot} . A sigmoidal, symmetric curve is obtained for isodesmic assembly. In contrast, cooperative aggregation results in a transition at $x_{\text{tot}} = 1$, which becomes sharper for smaller values of the cumulative cooperativity σ^{n-1} .⁴¹ The critical transition at $x_{\text{tot}} = 1$ implies that cooperative growth only occurs beyond a critical concentration and below a critical temperature. Next to the onset of the temperature- or concentration-dependent aggregation process, nucleation also influences the equilibrium length of the assemblies. While isodesmic assembly yields many relatively short chains, an unfavorable nucleation event results in a few assemblies with much larger length, since monomer addition to long aggregates is preferred over the nucleation of new, short assemblies.³⁹ This implies that the formation of long fibers or crystals, such as shown in Figures 3–5, is likely to originate from a nucleation step.

Kinetics of Single Nucleated Aggregation Pathways.

In the initial stages of a cooperative self-assembly process that results in long 1D fibers or crystals, nucleation has to take place before the first elongated structures can be formed. As the formation of a nucleus is an unfavorable event, the formation of

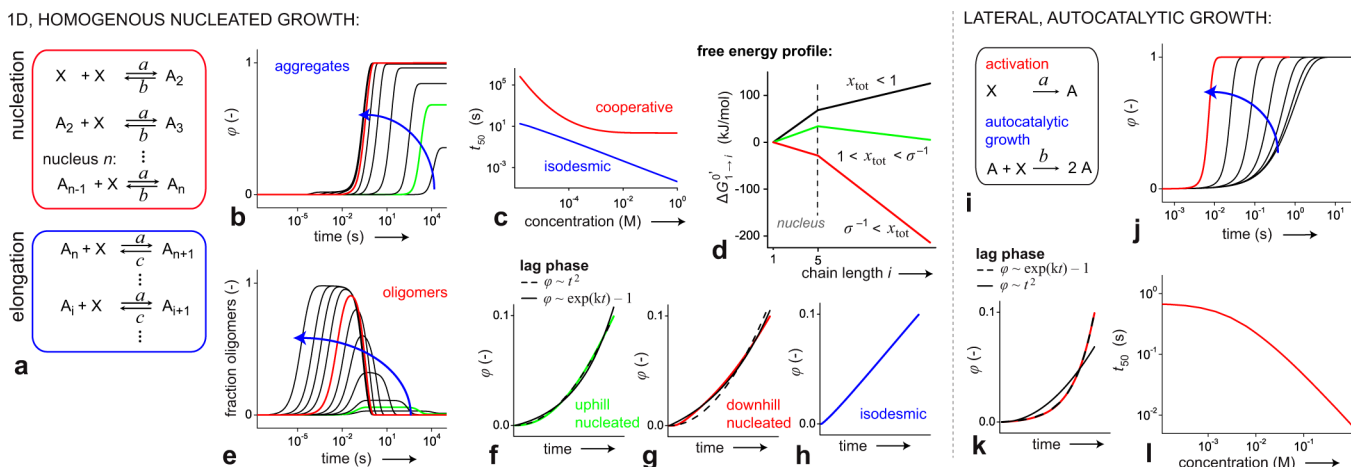


Figure 8. Analysis of assembly kinetics along a single pathway, assuming homogeneous nucleated (left, a) and lateral, autocatalytic (right, i) growth. Simulations performed for homogeneous nucleated growth ($a = 10^4 \text{ M}^{-1} \text{ s}^{-1}$, $b = 1 \text{ s}^{-1}$, $c = 0.01 \text{ s}^{-1}$, $n = 5$) show faster growth at higher concentration (b), although the rate levels off at high concentration (c) due to accumulation of material in prenucleus oligomers (e). For low concentration ($3.2 \mu\text{M}$, f), the lag phase can be described with a quadratic relation $\varphi \sim t^2$, whereas this approximation fails for high concentration (1.8 mM , g). This behavior corresponds to uphill and downhill nucleation, as depicted in the free energy profiles at 298 K (d). Isodesmic growth ($a = 10^4 \text{ M}^{-1} \text{ s}^{-1}$, $b = c = 0.01 \text{ s}^{-1}$) results in a monotonic decrease of t_{50} with concentration (c) and no lag phase (h). For lateral growth simulated with the phenomenological model developed by Finke and Watzky (i, $a = 1 \text{ s}^{-1}$, $b = 10^3 \text{ M}^{-1} \text{ s}^{-1}$), the rate increases monotonically with concentration (j, l) and the lag phase can be approximated with an exponential relation $\varphi \sim \exp(k \cdot t) - 1$ (k). The blue arrows indicate increasing concentration.

the initial aggregates is relatively slow. However, when more nuclei and large aggregates appear, further growth can take place more rapidly since monomer association is more favorable in the elongation regime. As a result, the initial rate of the aggregation increases after $t = 0$, resulting in a lag phase in the time-dependent degree of aggregation for a cooperative assembly process.⁴² Next to the critical temperature and concentration, such a lag phase is a hallmark for cooperative growth. It should be mentioned however that also pseudo lag phases can be observed for isodesmic systems if the experimental method is not sensitive to aggregates below a certain threshold size.⁴³

The previously introduced 1D and lateral growth processes have different nucleation mechanisms. In a 1D process, the growth in the initial phases of the process is dominated by monomer, nucleus, and eventually prenucleus species and can be considered as homogeneously nucleated growth.⁴⁴ For lateral growth, different nucleation pathways are involved as the surface of existing stacks nucleates the formation of new stacks. As a consequence of this secondary or heterogeneous nucleation, the aggregates catalyze their own formation (i.e., autocatalytic growth).⁴⁵ Here, we will analyze two models that describe 1D and lateral growth.

1D, Homogeneous Nucleated Growth Kinetics.

Recently, we started with studies focusing on the cooperative 1D assembly kinetics of molecular systems. Most theories employed to analyze fiber growth kinetics are originally developed to describe protein aggregation pathways involved in the formation of actin filaments or amyloid fibrils related to diseases like Alzheimers.⁴⁶ In our analysis, an insightful kinetic model developed by Powers and Powers⁴⁴ formed the basis of our approach, and we modified it as pointed out in ref 47. Analogous to the equilibrium model, the model describes the growth of 1D assemblies in a single pathway as a sequence of monomer addition steps. In the nucleation part of this mechanism, oligomers can change size upon monomer association and dissociation, with rate constants a and b , respectively. Beyond the nucleus with size n , further elongation takes place with monomer association rate constant a , and monomer dissociation is described with rate constant c . The decrease in the dissociation rate for elongation (c) relative to nucleation (b) reflects the cooperative character of the mechanism. The equilibrium constants for nucleation K_n and elongation K_e are equal to a/b and a/c , respectively, and the cooperativity σ follows from c/b .

Kinetic simulations with the model as shown in Figure 8a are performed by numerically solving the system of differential equations that describe the subsequent monomer association and dissociation steps. Simulations performed for a cooperative system ($\sigma = 0.01$ and $n = 5$) show that indeed in the initial stages of the growth process a lag phase can be observed (Figure 8f). In contrast, such a lag phase is absent in simulations assuming isodesmic growth (i.e., $\sigma = 1$, Figure 8h). Remarkable enough, the time at which 50% of the monomers are assembled into aggregates (t_{50}) levels off at the highest concentrations for a cooperative system ($\sigma = 0.01$ and $n = 5$), as shown in Figure 8c. Analogous simulations assuming isodesmic growth ($\sigma = 1$) do not show such a concentration independence at high concentrations. The leveling off of t_{50} at high concentrations for cooperative 1D aggregation is related to the formation of prenucleus oligomers:^{44,48} following the time-dependent fraction of material assembled in oligomers up to the nucleus size shows that for the highest concentrations a

significant amount of material is accumulated in prenucleus assemblies (Figure 8e). In the high concentration regime, the conversion rate from these oligomers to elongated assemblies becomes concentration-independent. Again, this phenomenon can also be observed for isodesmic systems if the smallest species are not captured by the experimental assay.

Lateral, Heterogeneous Nucleated Growth Kinetics.

To describe lateral growth, a minimalistic, phenomenological model has been developed by Finke and Watzky et al.^{45,49} First, the conversion of monomer X into aggregated state A is defined with activation rate constant a . Next, X reacts with A to yield 2 A, with rate constant b . As $b > a$, A enhances its own formation in an autocatalytic fashion (Figure 8i). Also in this mechanism, the resulting kinetic curves display a lag phase (Figure 8k). Besides, the rate increases monotonically with concentration (Figure 8j,l), unless the concentration is very low and formation of A takes mainly place via the monomolecular activation.

Unraveling Lag Phases in Nucleation Pathways. Since the lag phase is one of the characteristics of cooperative assembly, special attention is paid to the early stages of the aggregation process, both for homogeneous and heterogeneous nucleation. To this end, we focus first on the description of cooperative assembly via Gibbs free energy profiles. We start from the well-known equation $\Delta G^0 = -RT \ln(K)$, where K equals the equilibrium constant in M^{-1} , i.e., K_n in the nucleation regime and K_e in the elongation regime. It can be shown that for the dimensionless concentration x_{tot} which equals $K c_{\text{tot}} - RT \ln(x_{\text{tot}}) = -RT \ln(K) - RT \ln(c_{\text{tot}})$ holds. If we now define a new Gibbs free energy $\Delta G^{0'}_{i \rightarrow i+1}$ that equals $-RT \ln(x_{\text{tot}})$, the free energy profile can be constructed, i.e., $\Delta G^{0'}_{1 \rightarrow i}$ as a function of chain length i , starting with $\Delta G^{0'} = 0$ for the monomer. As shown in Figure 8d, the free energy profile is concentration-dependent. Formally, here the total concentration c_{tot} is taken as the reference state, whereas the standard state is defined at 1 M.⁵⁰ Three concentration regimes can now be recognized:⁴⁴ (1) If $x_{\text{tot}} < 1$, the free energy keeps increasing with chain length. Hence, the monomer is the lowest energy species, and no aggregation takes place in agreement with the simulations employing the equilibrium model. (2) If $1 < x_{\text{tot}} < \sigma^{-1}$, the nucleus is the highest energy species, but $\Delta G^{0'}_{1 \rightarrow i}$ decreases after the nucleus and hence elongation can take place. (3) If $x_{\text{tot}} > \sigma^{-1}$, the monomer is the highest energy species. A clear difference between the second and third regime is the development of $\Delta G^{0'}$ during the nucleation phase, which is uphill for regime (2) and downhill for regime (3). Hence, the formation of prenucleus oligomers is unfavorable in regime (2), whereas significant amounts of oligomeric species appear in the initial stages of the aggregation process for regime (3), as demonstrated in the kinetic simulations (Figure 8e).

In the case of homogeneous uphill nucleation, monomer and nucleus are the most dominant species during nucleation. This means that the rate in the initial stages of the aggregation (up to 10% conversion) can be approximated by $d\varphi/dt \sim k \cdot [\text{monomer}][\text{nucleus}]$. It can be shown that under these conditions the lag phase can be described by the quadratic relation $\varphi(t) \sim t^2$.^{51,52} For a homogeneous downhill aggregation, however, prenucleic oligomers cannot be neglected and therefore the lag phase does not have a quadratic dependence on time (Figure 8f,g).

If the aggregation process is dominated by lateral growth, the aggregation rate in the initial stages of the growth process is expected to be proportional to the amount of aggregated material present. Alternatively, also secondary nucleation effects

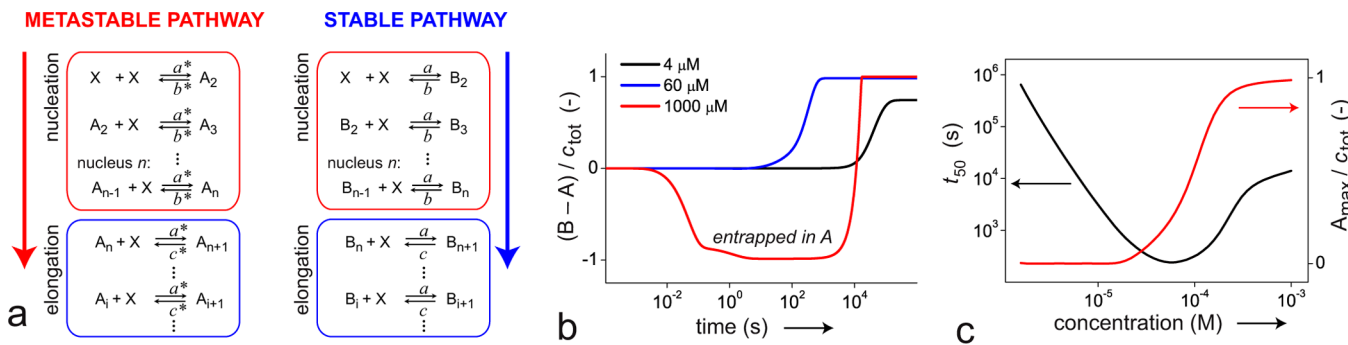


Figure 9. Analysis of assembly kinetics for a system that includes a metastable aggregation pathway. (a) Both the metastable and stable pathway—described via a sequence of monomer addition steps—compete for the same monomer X. (b) Kinetic simulations reveal that metastable assemblies (A) only appear at higher concentrations and result in the delay of the final formation of stable assemblies B. (c) Detailed analysis of the time at which 50% of the formation of the conversion toward stable B is complete (t_{50}) vs concentration shows that the concentration-rate relation becomes inverse around the concentration where significant amounts of A are initially formed, as represented by the maximum fraction of material entrapped in the metastable pathway in time, i.e., A_{\max}/C_{tot} . Parameters: $a^* = 10^6 \text{ M}^{-1} \text{ s}^{-1}$, $b^* = 1000 \text{ s}^{-1}$, $c^* = 10 \text{ s}^{-1}$, $a = 10^4 \text{ M}^{-1} \text{ s}^{-1}$, $b = 1 \text{ s}^{-1}$, $c = 0.01 \text{ s}^{-1}$, $K_e^* = 10^5 \text{ M}^{-1}$, $K_e = 10^6 \text{ M}^{-1}$, $\sigma^* = \sigma = 0.01$, $n = 5$.

PATHWAY COMPLEXITY:

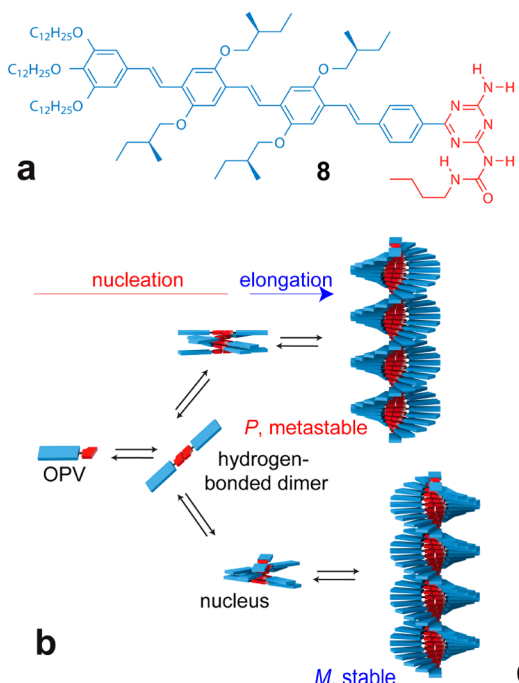


Figure 10. Pathway complexity and selection in the assembly of S-chiral oligo(*p*-phenylene vinylene) 8 (OPV, a). (b) Experiments under kinetic control reveal two nucleated pathways toward metastable, *P*-type and stable, *M*-type helices. (c) Starting from molecularly dissolved OPV at 70 °C, *P*-type helices are obtained upon quenching and *M*-type helices upon cooling with a rate of 1 °C/min, as evidenced by the CD spectra (100 μM). (d, e) Stopped-flow experiments reveal at low concentration (5–8 μM) a lag phase, and at higher concentrations (≥9 μM) the opposite CD intensity in the initial stages of the aggregation process (20 °C, CD followed at 466 nm). (f) t_{50} vs concentration reveals an inverted concentration–rate relation at higher concentrations, indicative of entrapment of material in the metastable pathway. (g) To obtain the metastable *P*-type assemblies exclusively, S-chiral dibenzoyl tartaric acid 9 (DTA) is attached to OPV via two-folded hydrogen bonding, resulting in *P*-type DTA–OPV assemblies. After extraction of DTA, *P*-type OPV assemblies are obtained exclusively, as evidenced by the CD intensity (h, 100 μM, 0 °C). (Reprinted with permission from ref 47. Copyright 2012 Nature Publishing Group.)

like fragmentation which facilitate formation of new nuclei are proportional to the degree of aggregation and hence intrinsically autocatalytic. Therefore, the aggregation rate in the initial stages of the nucleated growth can be approximated by $d\varphi/dt \sim k\cdot\varphi$. Hence, autocatalytic lag phases can be approximated by an exponential relation, i.e. $\varphi(t) \sim \exp(k\cdot t) - 1$, as shown in Figure 8k.^{51,52} In contrast, it is not possible to describe these lag phases with the quadratic scaling relation corresponding to homogeneous nucleation regime. Vice versa, the exponential

relation does not describe the lag phases obtained with the homogeneous nucleation model.

Kinetics of Aggregation Processes Including Metastable Pathways. The observation of several self-assembled pathways in the aggregation of π -conjugated materials, as illustrated by the examples discussed in Section 2, prompted us to analyze the consequences of multiple pathways that are competing for the same molecular building block by kinetic simulations. Again, we started our analysis with a model

developed by Powers and Powers,⁵³ which was modified to describe two cooperative pathways in parallel in a reversible fashion. Our model, introduced in ref 47, involves a metastable and a stable aggregation pathway that are both described as a sequence of monomer addition and dissociation steps (Figure 9a). The faster growth in the metastable pathway is expressed by its larger forward rate constant a^* compared to a , while the lower stability of this pathway finds its origin in the lower equilibrium constant of elongation K_e^* compared to K_e . An essential assumption in this model is that conversion from metastable to stable assemblies can only occur via the free monomer, i.e., by full disassembly of the metastable aggregate and subsequent growth of the equilibrium structure.

Simulations with the model show that metastable assemblies only appear in the initial stages of the growth process if the concentration is larger than $1/K_e^*$, i.e., well beyond the critical concentration of the metastable pathway (Figure 9b,c). Remarkably, also the time at which 50% of the aggregation process is completed (t_{50}) increases with concentration beyond this point. This can be rationalized by buffering of free monomers in metastable assemblies, which hampers subsequent formation of thermodynamically stable aggregates.

4. PATHWAY COMPLEXITY AND SELECTION

In our studies to unravel the assembly pathways of π -conjugated molecules, we use S-chiral oligo(*p*-phenylene vinylene) derivative 8 (OPV, Figure 10) as a model system.⁵⁴ This molecule consists of a π -conjugated oligo(*p*-phenylene vinylene) with chiral side chains, capped on one end by a tridodecylbenzene and on the other end by an ureidotriazine moiety. Because of the large π -system, OPV can easily be probed in diluted solution via spectroscopic techniques in the UV/vis regime, whereas the absence of turbidity or precipitation makes it possible to follow the entire aggregation process. The assembly pathway is initiated by self-complementary, fourfold hydrogen bonding, and in apolar solvents the resulting hydrogen-bonded OPV dimers aggregate into long one-dimensional helices. Due to the chiral side groups, one helicity is energetically favored over the other and hence the formation of these helices in solution can be probed with CD spectroscopy.

Cooperativity in OPV Assembly. To characterize the assembly mechanism of OPV in detail, temperature-dependent studies on OPV in the apolar solvent dodecane have been conducted by Jonkheijm et al.⁵⁵ At high temperatures, no CD effect is observed, and also the UV/vis and fluorescence spectra are comparable to those acquired in good solvent chloroform, indicative for molecularly dissolved, free OPV molecules and hydrogen-bonded dimers. At low temperatures, however, CD shows a bisignated, negative Cotton effect corresponding to left-handed, *M*-type helices. Concomitantly, UV/vis reveals a shoulder at 490 nm. Following CD during cooling at the wavelength where the maximum intensity can be observed, 466 nm, reveals a critical temperature at which the formation of helical assemblies starts, indicative of a cooperative growth process. However, the shoulder in UV/vis at 490 nm appears gradually upon cooling, prior to the critical transition in CD. Combining these spectroscopic data suggests that upon cooling initially small, disordered aggregates are formed that result in a shoulder in UV/vis at 490 nm but are CD silent as they have no helical organization. Only after the formation of a nucleus that contains multiple (i.e., more than two) hydrogen-bonded

dimers, a helical twist is introduced in the assembly and further elongation takes place more favorably.⁵⁶

Unraveling Pathway Complexity in OPV Assembly. To further unravel the assembly pathways of OPV, we recently designed an experiment to probe its assembly process in time.⁴⁷ The aggregation is induced by a transfer of OPV from chloroform, in which the OPV molecules and hydrogen-bonded dimers are molecularly dissolved, to an excess of poor solvent in which they assemble, methylcyclohexane (MCH). The subsequent formation of helical stacks is probed in CD, and the mixing of OPV in chloroform and MCH is performed using a stopped-flow (SF) setup, which enabled us to measure the kinetics with CD immediately after the transfer from good to poor solvent. Kinetic experiments conducted at 20 °C and low concentrations reveal a lag phase, in agreement with a cooperative growth mechanism (Figure 10d,e). At these low concentrations, the time-dependent CD is always negative, suggesting a direct formation of left-handed *M*-type assemblies. However, at higher concentrations, a positive CD signal appears in the initial stage of the aggregation process, indicative for the formation of metastable assemblies with opposite helicity (*P*-type). Also quenching from the molecular dissolved state at high temperature in MCH to 0 °C results in an opposite CD spectrum, whereas slow cooling with a rate of 1 °C/min yields the CD spectrum corresponding to the equilibrium aggregates (Figure 10c). Furthermore, entrapment of monomers in this metastable pathway results at high concentration in an inverted dependence of t_{50} on concentration (Figure 10f), similar to the effect simulated with the two-pathway kinetic model in Figure 9.

Pathway Selection: Isolating a Metastable Helical Structure. The experiments under kinetic control provide an elegant approach to reveal metastable pathways involved in the assembly of OPV. However, the low CD intensity of this metastable state obtained in the SF experiment and upon quenching suggests the formation of a mixture of *M*-type and *P*-type helices with the latter in small excess. To exclusively select the pathway resulting in metastable *P*-type helices, a two-step noncovalent synthetic method is developed by George et al. (Figure 10g).⁴⁷ First, S-chiral dibenzoyl tartaric acid (DTA, 9) is attached to the OPV hydrogen-bonded dimer at high temperature via twofold hydrogen bonding. Upon cooling, the DTA auxiliary dictates its chirality to OPV and thereby forces it to form assemblies with opposite helicity. In the second step, DTA is removed again from the OPV helices by aqueous extraction at 0 °C. Via this approach, exclusive formation of metastable *P*-type helices is obtained, as evidenced by the absolute magnitude of the CD spectrum at 0 °C that equals the CD magnitude of *M*-type helices under equilibrium conditions (Figure 10h). The metastable character of these *P*-type helices is demonstrated by a full conversion into *M*-type helices upon annealing at 25 °C.

Control over Dynamics by Selecting Solvent Conditions. Recently we demonstrated that both the assembly rate as well as the stability of the aggregates can be tuned by the ratio between good and poor solvent.⁵⁷ Stepwise addition of volume fractions (f) of OPV in chloroform to OPV assemblies in MCH results in disassembly profiles that can be described by assuming a free energy relation between the Gibbs free energy in the pure solvent and the mixed solvent. Moreover, stepwise increasing the chloroform content reveals a critical chloroform volume fraction f_{crit} at which the assemblies are fully disassembled. This critical solvent fraction is another hallmark

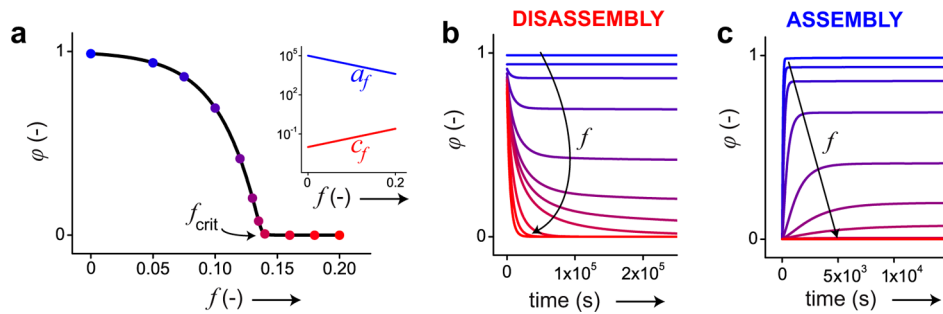


Figure 11. Simulated disassembly and assembly kinetics upon increasing volume fractions of cosolvent (f). (a) For a cooperative system, the degree of aggregation ϕ under equilibrium conditions vs cosolvent volume fraction f reveals a critical point at f_{crit} . (b, c) Kinetic simulations with a rate constant of monomer addition a that decreases with f and a rate constant of monomer dissociation c that increases with f (inset a) reveal both for disassembly and assembly minimum rates close to the critical volume fraction of cosolvent. Parameters: $a = 10^5 \text{ M}^{-1} \text{ s}^{-1}$, $c = 0.01 \text{ s}^{-1}$, $m_a = m_c = 7$, $n = 5$, $\sigma = 0.1$, $c_{\text{tot}} = 10 \mu\text{M}$.

of cooperativity in one-dimensional aggregation. Furthermore, the rate of the disassembly process, induced by the addition of chloroform to OPV assemblies in MCH, revealed a minimum rate close to the critical chloroform fraction. We attempted to rationalize the minimum rate around f_{crit} by introducing solvent-dependent rate constants in the single pathway kinetic model using a phenomenological relation. Therefore, the forward and backward rate constants a_f and c_f are defined via $\log(a_f) = \log(a) - m_a f$ and $\log(c_f) = \log(c) + m_c f$, respectively, where a and c represent the rate constants in pure MCH. The equilibrium constants in pure MCH are defined via $K_e = a/c$ and $K_n = \sigma \cdot K_e$. To simulate the disassembly kinetics, first the equilibrium concentrations of all species are calculated in pure MCH. Using these concentrations, the time-dependent disassembly is simulated with different values of f and rate constants adjusted to the respective volume fraction of chloroform, as shown in Figure 11. A minimum disassembly rate is obtained around f_{crit} , in agreement with the experimental observations. Furthermore, simulations of the reverse process, i.e., de novo nucleation of assemblies, reveal a minimum rate close to the critical solvent composition as well. Cooperativity turns out to be the key parameter in this phenomenon, as these effects cannot be simulated with isodesmic systems that obviously lack a critical solvent composition.

Since the rate of the aggregation process is a critical aspect in the selection of the desired pathway, different methodologies have been reported in literature for the transfer from good to poor solvent, varying from fast injection to (slow) vapor diffusion, as introduced in paragraph 2.⁵⁸ However, the kinetic experiments discussed here show that further control can be obtained by tuning the assembly rate via composition of the solvent itself. On the other hand, the nonlinear relation between the composition of the system and its dynamics can lead to counterintuitive consequences for the time-dependent aggregation process. For instance, inhomogeneous addition of a molecular building block in a good solvent to the system can result in a disassembly overshoot of the initially formed structures in solution. As a result, only full understanding of the possibilities to manipulate the rate of assembly processes by addition of a destabilizing cosolvent will extend the toolbox to control the aggregation pathways of π -conjugated materials.

5. CONCLUSION AND OUTLOOK

Control over the aggregation pathways will highly advance the development of functional π -conjugated materials. In some cases, post-treatments like annealing allow the molecules to

reorganize in the material.^{59,60} In other cases, however, the molecules are entrapped into a morphology that is determined by the conditions during processing from solution, even though this morphology is not the most stable one. Here, aggregation processes that start in the solution phase are critical for the pathway selected. Hence, numerous reports in literature show that the influence of aggregation in solution is widely appreciated, as illustrated by a variety of different evaporation and solvent transfer techniques,^{61–64} and by studies in which the addition of cosolvents such as diiodooctane during the spin coating of BHJ solar cells is varied in order to optimize the efficiency.^{65–69} However, these methods are all dominated by trial-and-error attempts, and further control over aggregation in solution can only be achieved by taking advantage of the mechanistic insights in assembly. The first step is to identify the different aggregates (i.e., states) involved in the system, via experiments under kinetic control like cooling with different temperature ramps or SF experiments. Having identified these states, the next step is to unravel the pathways, starting from the free monomer, toward these aggregates. To make a start with this, we demonstrated that competition between different pathways can be revealed by an inverse rate-concentration relation, due to entrapment of monomers in the metastable pathway at high concentrations. Even though analyses like these still require numerous experiments, we foresee that the development of processing methodologies via a model-driven approach will reduce the iterations that are required to arrive at the optimal nanoscale organization.

■ AUTHOR INFORMATION

Corresponding Author

*E-mail: e.w.meijer@tue.nl (E.W.M.).

Notes

The authors declare no competing financial interest.

Biographies

Peter Korevaar studied Chemical Engineering and Chemistry at the Eindhoven University of Technology and obtained his Master's degree in 2010. In February 2010, he started as a PhD student under supervision of Prof. Dr. Bert Meijer and Dr. Tom de Greef in the Institute for Complex Molecular Systems at the same university. He is interested in aggregation pathways involved in self-assembly processes, studied both via kinetic experiments as well as via the development of kinetic models.

Tom de Greef studied Biomedical Engineering at the Eindhoven University of Technology and continued with a PhD in Chemistry

(2009) in the group of Prof. E. W. Meijer and Prof. R. P. Sijbesma at the same university. In 2010 he was appointed assistant professor in the Computational Biology group and the Institute for Complex Molecular Systems. His research interests range from understanding the fundamental aspects of self-assembly to the forward engineering of complex biochemical systems.

E. W. "Bert" Meijer is a distinguished university professor and professor of organic chemistry at the Eindhoven University of Technology. He obtained his PhD in organic chemistry with Prof. Dr. Hans Wynberg from the University of Groningen in 1982. He then joined Philips Research Laboratories, and in 1989 he moved for three years to DSM Research. In 1991 he was appointed in Eindhoven. His research interests are focused on multistep noncovalent synthesis and the many challenges in functional supramolecular systems.

ACKNOWLEDGMENTS

We acknowledge financial support from the European Research Council (FP7/2007-2013) ERC Grant Agreement, funding from the Ministry of Education, Culture and Science (Gravity program 024.001.035), and The Netherlands Organization for Scientific Research (NWO; VENI Grant: 722.012.001 (T.F.A.d.G.)).

REFERENCES

- (1) Henson, Z. B.; Müllen, K.; Bazan, G. C. *Nat. Chem.* **2012**, *4*, 699.
- (2) Beaujuge, P. M.; Fréchet, J. M. *J. Am. Chem. Soc.* **2011**, *133*, 20009.
- (3) Greatzel, M.; Janssen, R. A. J.; Mitzi, D. B.; Sargent, E. H. *Nature* **2012**, *488*, 304.
- (4) Hoeben, F. J. M.; Jonkheijm, P.; Meijer, E. W.; Schenning, A. P. H. *J. Chem. Rev.* **2005**, *105*, 1491.
- (5) Mei, J.; Diao, Y.; Appleton, A. L.; Fang, L.; Bao, Z. *J. Am. Chem. Soc.* **2013**, *135*, 6724.
- (6) Rand, B. P.; Cheyns, D.; Vasseur, K.; Giebink, N. C.; Mothy, S.; Yi, Y.; Coropceanu, V.; Beljonnie, D.; Cornil, J.; Brédas, J.-L.; Genoe, J. *Adv. Funct. Mater.* **2012**, *22*, 2987.
- (7) Aiyar, A. R.; Hong, J.-I.; Reichmanis, E. *Chem. Mater.* **2012**, *24*, 2845.
- (8) Rahimi, K.; Botiz, I.; Stigelin, N.; Kayunkid, N.; Sommer, M.; Koch, F. P. V.; Nguyen, H.; Coumbier, O.; Dubois, P.; Brinkmann, M.; Reiter, G. *Angew. Chem., Int. Ed.* **2012**, *51*, 11131.
- (9) Gentili, D.; Di Maria, F.; Liscio, F.; Ferlauto, L.; Leonardi, F.; Maini, L.; Gazzano, M.; Milita, S.; Barbarella, G.; Cavallini, M. *J. Mater. Chem.* **2012**, *22*, 20852.
- (10) Treat, N. D.; Nekuda Malik, J. A.; Reid, O.; Yu, L.; Shuttle, C. G.; Rumbles, G.; Hawker, C. J.; Chabiny, M. L.; Smith, P.; Stigelin, N. *Nat. Mater.* **2013**, *12*, 628.
- (11) Ajayaghosh, A.; Varghese, R.; Praveen, V. K.; Mahesh, S. *Angew. Chem., Int. Ed.* **2006**, *45*, 3261.
- (12) Tidhar, Y.; Weissman, H.; Wolf, S. G.; Gulino, A.; Rybtchinski, B. *Chem.—Eur. J.* **2011**, *17*, 6068.
- (13) Wolffs, M.; Korevaar, P. A.; Jonkheijm, P.; Henze, O.; Feast, W. J.; Schenning, A. P. H. J.; Meijer, E. W. *Chem. Commun.* **2008**, 4613.
- (14) Percec, V.; Sun, H.-J.; Leowanawat, P.; Peterca, M.; Graf, R.; Spiess, H. W.; Zeng, X.; Ungar, G.; Heiney, P. A. *J. Am. Chem. Soc.* **2013**, *135*, 4129.
- (15) Lakwani, G.; Meskers, S. C. J. *Macromolecules* **2009**, *42*, 4220.
- (16) Wedl, B.; Resel, R.; Leising, G.; Kunert, B.; Salzmann, I.; Oehzelt, M.; Koch, N.; Vollmer, A.; Duhm, S.; Werzer, O.; Gbabode, G.; Sferrazza, M.; Geerts, Y. *RSC Adv.* **2012**, *2*, 4404.
- (17) Gopal, A.; Varghese, R.; Ajayaghosh, A. *Chem. Asian J.* **2012**, *7*, 2061.
- (18) Lin, Z.-Q.; Sun, P.-J.; Tay, Y.-Y.; Liang, J.; Liu, Y.; Shi, N.-E.; Xie, L.-H.; Yi, M.-D.; Qian, Y.; Fan, Q.-L.; Zhang, H.; Hng, H. H.; Ma, J.; Zhang, Q.; Huang, W. *ACS Nano* **2012**, *6*, 5309.
- (19) Mei, J.; Graham, K. R.; Stalder, R.; Tiwari, S. P.; Cheun, H.; Shim, J.; Yoshio, M.; Nuckolls, C.; Kippelen, B.; Castellano, R. K.; Reynolds, J. R. *Chem. Mater.* **2011**, *23*, 2285.
- (20) Yu, L.; Li, X.; Pavlica, E.; Koch, F. P. V.; Portale, G.; da Silva, I.; Loth, M. A.; Anthony, J. E.; Smith, P.; Bratina, G.; Kjellander, B. K. C.; Bastiaansen, C. W. M.; Broer, D. J.; Gelink, G. H.; Stigelin, N. *Chem. Mater.* **2013**, *25*, 1823.
- (21) Vakhshouri, K.; Gomez, E. D. *Macromol. Rapid Commun.* **2012**, *33*, 2133.
- (22) Dang, M. T.; Hirsch, L.; Wantz, G.; Wuest, J. D. *Chem. Rev.* **2013**, *113*, 3734.
- (23) Yao, Y.; Dong, H.; Hu, W. *Polym. Chem.* **2013**, DOI: 10.1039/c3py00131h.
- (24) Bouman, M. M.; Meijer, E. W. *Adv. Mater.* **1995**, *7*, 385.
- (25) Satrijo, A.; Meskers, S. C. J.; Swager, T. M. *J. Am. Chem. Soc.* **2006**, *128*, 9030.
- (26) Satrijo, A.; Swager, T. M. *Macromolecules* **2005**, *38*, 4054.
- (27) Tevis, I. D.; Palmer, L. C.; Herman, D. J.; Murray, I. P.; Stone, D. A.; Stupp, S. I. *J. Am. Chem. Soc.* **2011**, *133*, 16486.
- (28) Stone, D. A.; Tayi, A. S.; Goldberger, J. E.; Palmer, L. C.; Stupp, S. I. *Chem. Commun.* **2011**, *47*, 5702.
- (29) Giri, G.; Verploegen, E.; Mannsfeld, S. C. B.; Atahan-Evrenk, S.; Kim, D. H.; Lee, S. Y.; Becerril, H. A.; Aspuru-Guzik, A.; Toney, M. F.; Bao, Z. *Nature* **2011**, *480*, 504.
- (30) Hill, J. P.; Jin, W.; Kosaka, A.; Fukushima, T.; Ichihara, H.; Shimomura, T.; Ito, K.; Hashizume, T.; Ishii, N.; Aida, T. *Science* **2004**, *304*, 1481.
- (31) Jin, W.; Fukushima, T.; Niki, M.; Kosaka, A.; Ishii, N.; Aida, T. *Proc. Natl. Acad. Sci. U.S.A.* **2005**, *102*, 10801.
- (32) Yamamoto, T.; Fukushima, T.; Yamamoto, Y.; Kosaka, A.; Jin, W.; Ishii, N.; Aida, T. *J. Am. Chem. Soc.* **2006**, *128*, 14337.
- (33) Würthner, F.; Yao, S.; Beginn, U. *Angew. Chem., Int. Ed.* **2003**, *42*, 3247.
- (34) Lohr, A.; Lysetska, M.; Würthner, F. *Angew. Chem., Int. Ed.* **2005**, *44*, 5071.
- (35) Lohr, A.; Würthner, F. *Angew. Chem., Int. Ed.* **2008**, *47*, 1232.
- (36) Ihn, K. J.; Moulton, J.; Smith, P. J. *Polym. Sci., Part B: Polym. Phys.* **1993**, *31*, 735.
- (37) Liu, J.; Arif, M.; Zou, J.; Khondaker, S. I.; Zhai, L. *Macromolecules* **2009**, *42*, 9390.
- (38) Takizawa, Y.; Shimomura, T.; Miura, T. *J. Phys. Chem. B* **2013**, *117*, 6282.
- (39) De Greef, T. F. A.; Smulders, M. M. J.; Wolffs, M.; Schenning, A. P. H. J.; Sijbesma, R. P.; Meijer, E. W. *Chem. Rev.* **2009**, *109*, 5687.
- (40) Zhao, D.; Moore, J. S. *Org. Biomol. Chem.* **2003**, *1*, 3471.
- (41) Goldstein, R. F.; Stryer, L. *Biophys. J.* **1986**, *50*, 583.
- (42) Frieden, C. *Protein Sci.* **2007**, *16*, 2334.
- (43) Roberts, C. J. *Biotechnol. Bioeng.* **2007**, *98*, 927.
- (44) Powers, E. T.; Powers, D. L. *Biophys. J.* **2006**, *91*, 122.
- (45) Morris, A. M.; Watzky, M. A.; Agar, J. N.; Finke, R. G. *Biochemistry* **2008**, *47*, 2413.
- (46) Morris, A. M.; Watzky, M. A.; Finke, R. G. *Biochim. Biophys. Acta* **2009**, *1794*, 375.
- (47) Korevaar, P. A.; George, S. J.; Markvoort, A. J.; Smulders, M. M. J.; Hilbers, P. A. J.; Schenning, A. P. H. J.; De Greef, T. F. A.; Meijer, E. W. *Nature* **2012**, *481*, 492.
- (48) Kodaka, M. *Biophys. Chem.* **2004**, *109*, 325.
- (49) Watzky, M. A.; Finke, R. G. *J. Am. Chem. Soc.* **1997**, *119*, 10382.
- (50) Xue, W.-F.; Homans, S. W.; Radford, S. E. *Proc. Natl. Acad. Sci. U.S.A.* **2008**, *105*, 8926.
- (51) Bishop, M. F.; Ferrone, F. A. *Biophys. J.* **1984**, *46*, 631.
- (52) Ferrone, F. A. *Methods Enzymol.* **1999**, *309*, 256.
- (53) Powers, E. T.; Powers, D. L. *Biophys. J.* **2008**, *94*, 379.
- (54) Schenning, A. P. H. J.; Jonkheijm, P.; Peeters, E.; Meijer, E. W. *J. Am. Chem. Soc.* **2001**, *123*, 409.
- (55) Jonkheijm, P.; Van der Schoot, P.; Schenning, A. P. H. J.; Meijer, E. W. *Science* **2006**, *313*, 80.
- (56) Kulkarni, C.; Balusubramanian, S.; George, S. J. *ChemPhysChem* **2013**, *14*, 661.

- (57) Korevaar, P. A.; Schaefer, C.; De Greef, T. F. A.; Meijer, E. W. *J. Am. Chem. Soc.* **2012**, *134*, 13482.
- (58) Zang, L.; Che, Y.; Moore, J. S. *Acc. Chem. Res.* **2008**, *41*, 1596.
- (59) Lilliu, S.; Agostinelli, T.; Pires, E.; Hampton, M.; Nelson, J.; Macdonald, J. E. *Macromolecules* **2011**, *44*, 2725.
- (60) Verploegen, E.; Miller, C. E.; Schmidt, K.; Bao, Z.; Toney, M. F. *Chem. Mater.* **2012**, *24*, 3923.
- (61) Kwak, D.; Lim, J. A.; Kang, B.; Lee, W. H.; Cho, K. *Adv. Funct. Mater.* **2013**, *12*, 665.
- (62) Diao, Y.; Tee, B. C.-K.; Giri, G.; Xu, J.; Kim, D. H.; Becerril, H. A.; Stoltzberg, R. M.; Lee, T. H.; Xue, G.; Mannsfeld, S. C. B.; Bao, Z. *Nat. Mater.* **2013**, *12*, 665.
- (63) Peet, J.; Sanetore, M. L.; Heeger, A. J.; Bazan, G. C. *Adv. Mater.* **2009**, *21*, 1521.
- (64) Wang, S.; Dössel, L.; Mavrinckiy, A.; Gao, P.; Feng, X.; Pisula, W.; Müllen, K. *Small* **2011**, *7*, 2841.
- (65) Sun, Y.; Welch, G. C.; Leong, W. L.; Takacs, C. J.; Bazan, G. C.; Heeger, A. J. *Nat. Mater.* **2012**, *11*, 44.
- (66) Rogers, J. T.; Schmidt, K.; Toney, M. F.; Bazan, G. C.; Kramer, E. J. *J. Am. Chem. Soc.* **2012**, *134*, 2884.
- (67) Cabanatos, C.; El Labban, A.; Bartelt, J. A.; Douglas, J. D.; Mateker, W. R.; Fréchet, J. M. J.; McGehee, M. D.; Beaujuge, P. M. J. *Am. Chem. Soc.* **2013**, *135*, 4656.
- (68) Zhou, H.; Zhang, Y.; Seifert, J.; Collins, S. D.; Luo, C.; Bazan, G. C.; Nguyen, T.-Q.; Heeger, A. J. *Adv. Mater.* **2013**, *25*, 1646.
- (69) Di Nuzzo, D.; Aguirre, A.; Shahid, M.; Gevaerts, V. S.; Meskers, S. C. J.; Janssen, R. A. J. *Adv. Mater.* **2010**, *22*, 4321.